Journal of Catalysis 268 (2009) 335–342

Contents lists available at ScienceDirect

Journal of Catalysis

journal homepage: www.elsevier.com/locate/jcat

Trend in the C=C and C=O bond hydrogenation of acrolein on Pt–M (M = Ni, Co, Cu) bimetallic surfaces

Luis E. Murillo [a,1], Carl A. Menning [b], Jingguang G. Chen [b,*]

[a] Department of Materials Science and Engineering, Center for Catalytic Science and Technology, University of Delaware, Newark, DE 19716, United States
[b] Department of Chemical Engineering, Center for Catalytic Science and Technology, University of Delaware, Newark, DE 19716, United States

ARTICLE INFO

Article history:
Received 9 July 2009
Revised 23 September 2009
Accepted 1 October 2009
Available online 31 October 2009

Keywords:
Bimetallic
Acrolein
Ni
Co
Cu
Pt(1 1 1)
Selective hydrogenation
TPD
HREELS
DFT

ABSTRACT

Acrolein, the smallest α,β-unsaturated aldehyde, is used as a probe molecule to study the effect on the hydrogenation activity toward the C=C and C=O bonds due to the presence of a 3d transition metal either on the surface or in the subsurface region of a Pt(1 1 1) substrate. Temperature programmed desorption (TPD), high-resolution electron energy loss spectroscopy (HREELS), and density functional theory (DFT) modeling are used to help explain the trend in the overall hydrogenation activity and selectivity toward the corresponding unsaturated alcohol (2-propenol) on the 3d/Pt(1 1 1) bimetallic surfaces. The hydrogenation activity on the subsurface Pt–3d–Pt(1 1 1) structures displays the following trend: Pt–Ni–Pt(1 1 1) > Pt–Co–Pt(1 1 1) > Pt–Cu–Pt(1 1 1) based on the TPD yields. The absolute yield toward 2-propenol is also the highest on Pt–Ni–Pt(1 1 1), which is further enhanced by the presence of pre-adsorbed hydrogen. In contrast, the selective hydrogenation does not occur on the surface monolayer 3d–Pt(1 1 1) structures. The TPD results are consistent with HREELS measurements of different vibrational features after the adsorption and reaction of acrolein on the subsurface Pt–3d–Pt(1 1 1) and surface 3d–Pt(1 1 1) structures. In addition, DFT calculations suggest that the different hydrogenation activities between the subsurface and surface structures appear to be related to the differences in the binding energy of acrolein on the corresponding bimetallic surfaces.

1. Introduction

The selective hydrogenation of α,β-unsaturated aldehydes to unsaturated alcohols has been of growing interest because unsaturated alcohols are important intermediates for the production of fine chemicals and pharmaceutical precursors. In addition, such studies also offer the opportunity to understand the origin of selective hydrogenation of molecules with multiple unsaturated functional groups [1–3].

Many attempts have been made to promote the selective hydrogenation of α,β-unsaturated aldehydes by taking advantage of the synergistic effects of using bimetallic catalysts. Galvagno et al. observed that the addition of Sn to the Ru/C catalyst increased the selective hydrogenation of citral toward nerol and genariol; however, the overall activity for the reaction was decreased. The addition of Sn was found to have two effects: the poisoning of the Ru sites that decreased the overall activity and the activation of the carbonyl group due to the presence of $Sn^{\delta+}$ ions [4]. Neri et al. studied the same reaction over Pt–Sn supported on activated carbon. By adding small amounts of Sn to the Pt catalysts, the selectivity to unsaturated alcohol was found to increase, reaching a maximum at Sn loadings of 0.30 wt.% with a fixed Pt loading of 2 wt.%. In this case, the overall hydrogenation activity was also increased [5]. Raab and Lercher studied the selective hydrogenation of crotonaldehyde on supported NiPt on SiO_2 [6] and TiO_2 [7], with SiO_2-supported bimetallic catalysts showing higher selectivity. However, the overall hydrogenation activity was the highest for the Ni/SiO_2 catalyst. The preferred activation of the C=O double bond on the bimetallic catalysts was attributed to the presence of negatively charged Pt and positively charged Ni [6]. Lucas and Claus recently reported that Ag–In supported on silica showed a conversion greater than 90% and a selectivity to 2-propenol around 60%, using a micro plug-flow reactor at 513 K and pressures higher than 2 MPa with H_2 to acrolein molar ratio around 20 [8]. In this case, the presence of partially reduced metals was found to be responsible for the enhancement in the hydrogenation of the carbonyl group since a di-σ-C–O adsorption configuration was preferred over these active polar sites [1,8].

In order to better understand the hydrogenation pathways of α,β-unsaturated aldehydes on catalysts without the effect of the catalyst support, fundamental studies on Pt single crystal and Pt-based bimetallic surfaces have been carried out by adding Sn to Pt(5 5 3) [9] and Sn, Fe, and Ni to Pt(1 1 1) [2,3,10–18]. For

* Corresponding author. Fax: +1 302 831 2085.
E-mail address: jgchen@udel.edu (J.G. Chen).
[1] Present address: DuPont, Experimental Station, ESL402/5211, Wilmington, DE 19880, United States.

0021-9517/$ - see front matter © 2009 Elsevier Inc. All rights reserved.
doi:10.1016/j.jcat.2009.10.003

example, recent results reported by our research group have suggested that the bimetallic Pt–Ni–Pt(1 1 1) surface, with Ni atoms residing in the second layer of the Pt(1 1 1) substrate, promoted the selective hydrogenation of acrolein toward the corresponding unsaturated alcohol under ultra-high vacuum (UHV) conditions [18,19]. The combined experimental and DFT results suggested that the presence of weakly adsorbed acrolein through a di-σ-C–O configuration appeared to be responsible for this desired hydrogenation pathway [18].

In the current paper we extend our studies to other 3d/Pt(1 1 1) bimetallic surfaces, including Co and Cu, to determine the general trend in the hydrogenation activity and selectivity of acrolein on subsurface Pt–3d–Pt(1 1 1) and surface 3d–Pt–Pt(1 1 1) structures. In addition to experimental studies using TPD and HREELS, DFT calculations are also performed to correlate the hydrogenation activity with the binding energy and adsorption geometry of acrolein on these bimetallic surfaces.

2. Experimental and DFT methods

A two-level stainless steel UHV chamber with a base pressure less than 1×10^{-10} Torr was used to carry out the TPD experiments. This UHV chamber has been described elsewhere [20]. In brief, bimetallic surfaces were prepared using a Pt(1 1 1) single crystal (Metal Crystals and Oxides, Ltd., Cambridge) as a substrate for the different 3d transition metals. This crystal was spot welded directly to two tantalum posts for resistive heating and thermal contacts for cooling with liquid nitrogen. The Pt(1 1 1) surface was prepared by cycles of sputtering, oxygen treatment, and annealing, as described previously [21]. The cleanliness of the surface was checked by Auger electron spectroscopy (AES). After dosing acrolein or hydrogen/acrolein at ~100 K, the TPD experiments were performed with the surface placed at a distance of ~5 mm from the opening of the random flux shield of the mass spectrometer. A heating rate of 3 K/s was used to a maximum of 800 K while collecting 10 masses simultaneously. The TPD yields were estimated by using the procedure reported by Ko et al. and the sensitivity factors relative to CO as explained in previous studies [19,22].

The vibrational spectroscopic measurements were carried out in a separate UHV chamber equipped with an LK-3000 double-pass HREEL spectrometer for vibrational analysis, as described previously [23,24]. The intensity of the elastic peak was in the range between 3×10^4 and 3×10^5 counts per second (cps) with a spectral resolution between 30 and 40 cm^{-1} full-width at half maximum (FWHM). The exposure of acrolein or hydrogen/acrolein was made with the Pt(1 1 1) or bimetallic 3d–Pt(1 1 1) surface held at <120 K. The initial spectrum was scanned at low temperature (110−120 K). The adsorbed layer was then annealed to a specific temperature with a linear rate of 3 K/s, held for 5 s, then cooled down to ~120 K for data collection.

Acrolein (Alfa Aesar, 99.9% stabilized with 0.1% hydroquinone) was purified by successive freeze–pump–thaw cycles prior to use. The purity was verified in situ by mass spectrometry. Hydrogen, oxygen, and neon were all of research grade purity (99.999%) and were introduced into the UHV chamber without further purification. Doses are reported in Langmuirs (1 Langmuir (L) = 1×10^{-10} Torr s) and are not corrected for ion gauge sensitivities. Acrolein, hydrogen, and oxygen were dosed through directional dosing tubes with a diameter of ~5 mm. For H_2 dosing, the exposure of 0.5 L in the TPD chamber and 5 L in the HREELS chamber resulted in ~50% saturation coverage of hydrogen.

As reported earlier for the Ni/Pt(1 1 1) system, a surface Ni–Pt–Pt(1 1 1) structure was prepared by depositing one monolayer (ML) of Ni at 300 K, while the subsurface Pt–Ni–Pt(1 1 1) structure was obtained by the deposition of one ML Ni at 600 K [25]. In the current study bimetallic surfaces were prepared by evaporating approximately one ML of 3d transition metal (Ni, Co, and Cu) on the Pt(1 1 1) surface by maintaining the crystal at 300 and 600 K to prepare the surface 3d–Pt–Pt(1 1 1) and subsurface Pt–3d–Pt(1 1 1) structures, respectively. The evaporative 3d metal doser consisted of a metal wire (at least 99.99% purity) wrapped around a resistively heated tungsten wire. This metal filament was enclosed in a stainless steel cylinder with an opening of ~1 cm in diameter. During the metal evaporation, the UHV pressure remained below 5×10^{-10} Torr. The metal coverage was estimated using AES by monitoring the 3d(LMM)/Pt(241 eV) AES peak-to-peak ratio.

Self-consistent periodic slab calculations were performed by density functional theory (DFT) using the code VASP (Vienna ab initio Simulation Package) [26]. A plane-wave basis set with a cutoff energy of 396 eV was used to solve the Kohn–Sham equations. The PW91 functional was utilized to describe the exchange correlation term. Vanderbilt ultrasoft pseudopotential was used to describe the core electrons and the nuclei of the atoms, as described previously [27,28]. The different electronic energies were calculated using a $3 \times 3 \times 1$ *k*-point grid mesh. The bimetallic surfaces were modeled using 3×3 super cells of four layers of thickness, which were separated by a vacuum region equivalent in thickness to six metal layers to prevent electronic interaction between slabs. The binding energy of acrolein was calculated with one acrolein molecule adsorbed per unit cell, with the top two metal layers allowed to relax. Calculations for gas-phase acrolein and adsorbate–metal systems were carried out spin-unpolarized, as described previously [18].

3. Results and discussion

3.1. TPD of acrolein on Pt–3d–Pt(1 1 1) and 3d–Pt–Pt(1 1 1) surfaces

3.1.1. Reaction products from Ni/Pt(1 1 1) surfaces

Fig. 1 shows the TPD spectra after the adsorption of 0.5 L acrolein, corresponding to a coverage near the saturation of the first monolayer, on Pt–Ni–Pt(1 1 1), H/Pt–Ni–Pt(1 1 1) (representing Pt–Ni–Pt(1 1 1) with ~50% saturation coverage of pre-adsorbed hydrogen), Ni–Pt–Pt(1 1 1), and Pt(1 1 1). The TPD results on these surfaces have been described previously [18,19]; they are shown here to provide a reference to compare with other Pt–3d–Pt(1 1 1) and 3d–Pt–Pt(1 1 1) surfaces. In brief, masses characteristic of different desorption products are compared in Fig. 1, including hydrogen (H_2, 2 amu), carbon monoxide (CO, 28 amu), molecular desorption of acrolein (CH_2=CH–CH=O, 56 amu), 1-propanol (CH_3–CH_2–CH_2–OH, 60 amu), propanal (CH_3–CH_2–CH=O, 58 amu), and 2-propenol (CH_2=CH–CH_2–OH, 31 amu). Consistent with that observed by Zaera et al., acrolein undergoes mainly decarbonylation on the Pt(1 1 1) surface [29]. No noticeable desorption features are observed from 31, 58, or 60 amu from Pt(1 1 1). In comparison, both propanal and 2-propenol are detected at 272 K from the Pt–Ni–Pt(1 1 1) surface. When acrolein is adsorbed on the hydrogen pre-dosed H/Pt–Ni–Pt(1 1 1) surface, a small desorption peak of 1-propanol is observed at 268 K, and the desorption of propanal at 193 and 272 K and 2-propenol at 272 K is enhanced due to the presence of pre-adsorbed hydrogen. The molecular desorption of acrolein is noticeable from both Pt–Ni–Pt(1 1 1) and H/Pt–Ni–Pt(1 1 1). On the Ni–Pt–Pt(1 1 1) surface, the molecular desorption of acrolein occurs at 190 K, and a desorption peak of propanal is observed at 302 K and a very weak peak of 2-propenol is detected at 304 K.

3.1.2. Reaction products from Co/Pt(1 1 1) surfaces

The TPD spectra after the exposure of 0.5 L acrolein on different Co/Pt(1 1 1) surfaces are displayed in Fig. 2. The characterization of

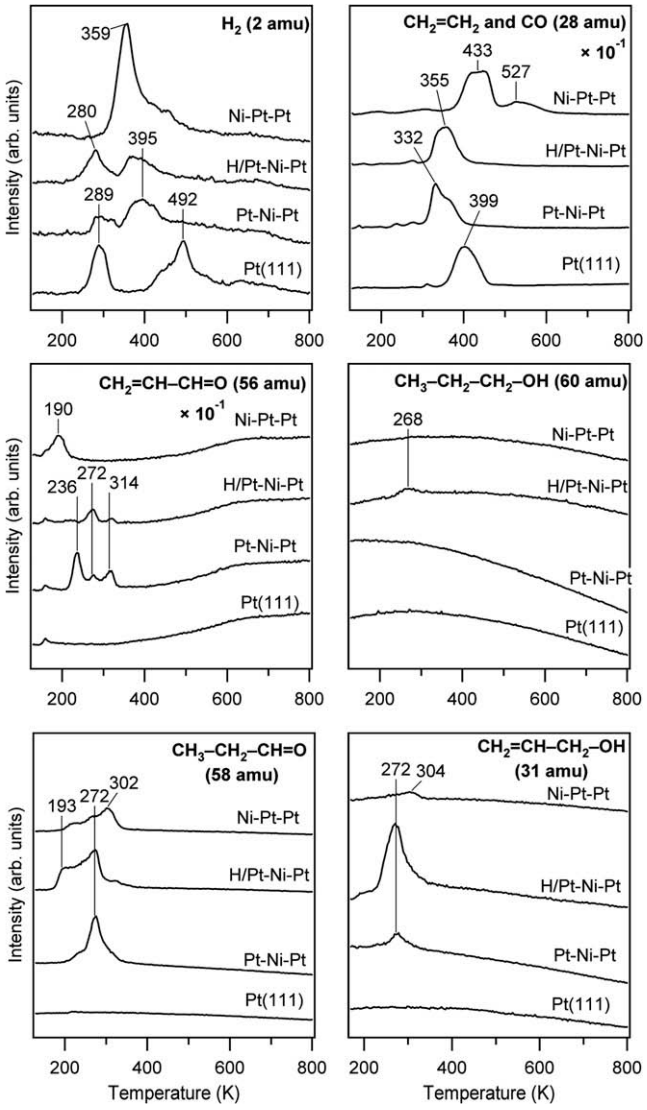

Fig. 1. TPD spectra of the reaction products of acrolein from Pt(1 1 1), Pt–Ni–Pt(1 1 1), H/Pt–Ni–Pt(1 1 1), and Ni–Pt–Pt(1 1 1) surfaces after dosing 0.5 L acrolein. The characteristic cracking patterns are: 2 amu (hydrogen); 28 amu (CO and ethylene); 56 amu (acrolein); 60 amu (1-propanol); 58 amu (propanal); and 31 amu (2-propenol).

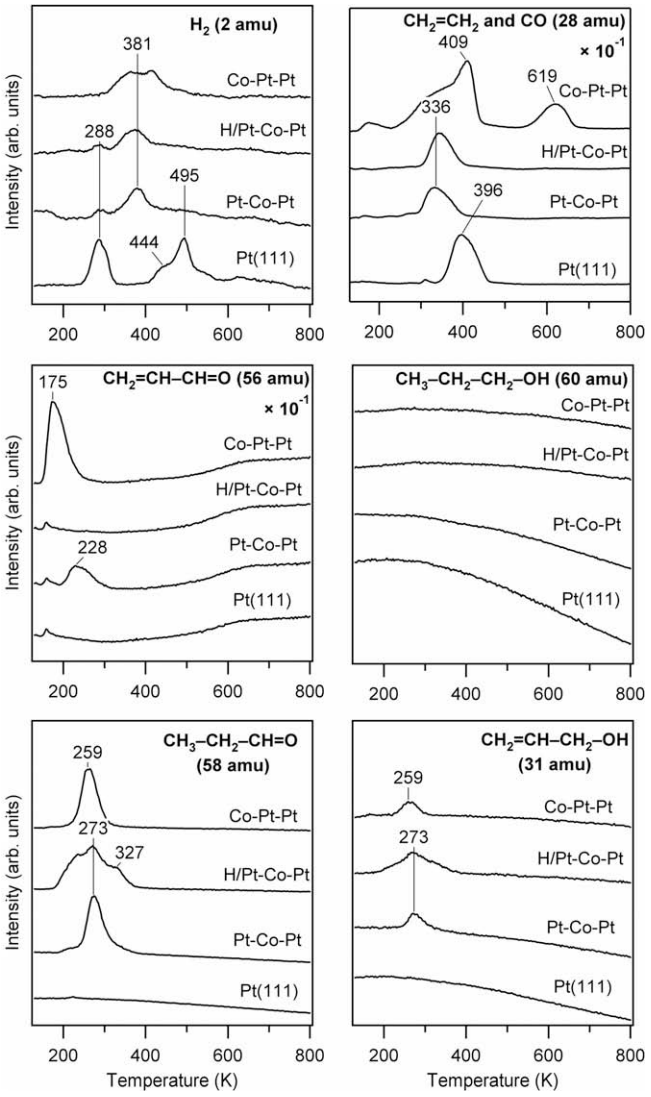

Fig. 2. TPD spectra of the reaction products of acrolein from Pt(1 1 1), Pt–Co–Pt(1 1 1), H/Pt–Co–Pt(1 1 1), and Co–Pt–Pt(1 1 1) surfaces after dosing 0.5 L acrolein. The characteristic cracking patterns are: 2 amu (hydrogen); 28 amu (CO and ethylene); 56 amu (acrolein); 60 amu (1-propanol); 58 amu (propanal); and 31 amu (2-propenol).

the Co/Pt(1 1 1) surface structures has been described in the literature by different groups using LEED, STM, AES, UPS, and hydrogen TPD [30–33]. Similar diffusion of Co atoms to the subsurface of Pt(1 1 1), as the one described for the Pt–Ni–Pt(1 1 1) surface [25,34], has been reported to occur when Co is deposited at 600 K [31–33]. Correspondingly, an enriched Co surface layer on Pt(1 1 1) can be prepared when Co is evaporated at a substrate temperature of 300 K [30,31,33]. As shown in Fig. 2, the desorption of the H_2 product from the Pt–Co–Pt(1 1 1) surface takes place at 288 and 381 K, with the desorption of the CO product occurring at ~336 K. Acrolein desorbs molecularly at 228 K. The desorption of both propanal and 2-propenol occurs at a peak centered at 273 K. Pre-adsorbed hydrogen on the Pt–Co–Pt(1 1 1) surface leads to an enhancement in the production of both propanal and 2-propenol. In comparison, from the Co–Pt–Pt(1 1 1) surface the H_2 and CO products desorb at higher temperatures, with CO desorbing at 409 and 619 K. The molecular desorption of acrolein is observed as a relatively sharp peak at 175 K. Finally, hydrogenated products, propanal and a smaller amount of 2-propenol, are detected at 259 K from this surface.

3.1.3. Reaction products from Cu/Pt(1 1 1) surfaces

The deposition of Cu on Pt(1 1 1) at around 350 K was studied using LEED and AES by Tsay et al. [35]. At this temperature, a Cu film on top of the Pt(1 1 1) substrate was suggested to be formed [35]. In the experiments mentioned here, deposition was carried out at 300 K for up to 1 ML based on AES measurements. When Cu is deposited at 600 K, the diffusion of Cu atoms to the bulk is suggested from AES measurements. However, previous studies proposed that the formation of a Cu–Pt alloy takes place when Cu is deposited at 350 K and then annealed to 600–700 K [35]. For consistency with the other 3d/Pt(1 1 1) bimetallic structures, this surface is referred to as a Pt–Cu–Pt(1 1 1) structure in the current study.

The TPD spectra after the adsorption of 0.5 L acrolein on Cu/Pt(1 1 1) surfaces are displayed in Fig. 3. The H_2 and CO products desorb from the Pt–Cu–Pt(1 1 1) surface at 452 K and 360 K, respectively. The desorption of propanal occurs at 270 K, with a very weak peak of 2-propenol occurring at the same temperature. The presence of pre-adsorbed hydrogen on Pt–Cu–Pt(1 1 1) does not enhance the desorption of either propanal or 2-propenol. On

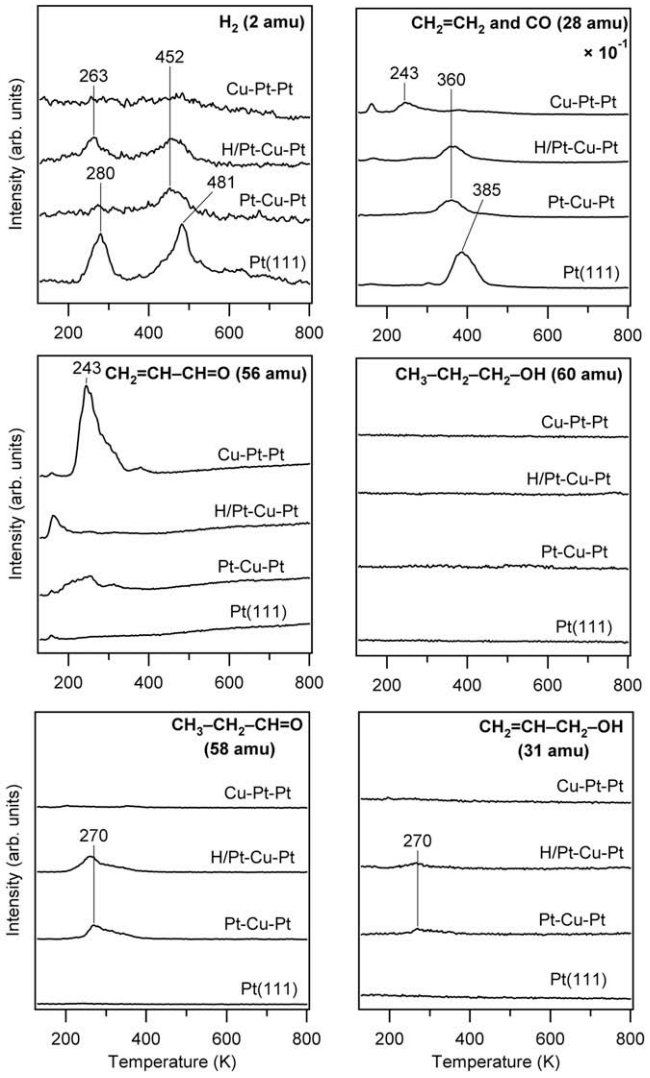

Fig. 3. TPD spectra of the reaction products of acrolein from Pt(1 1 1), Pt–Cu–Pt(1 1 1), H/Pt–Cu–Pt(1 1 1), and Cu–Pt–Pt(1 1 1) surfaces after dosing 0.5 L acrolein. The characteristic cracking patterns are: 2 amu (hydrogen); 28 amu (CO and ethylene); 56 amu (acrolein); 60 amu (1-propanol); 58 amu (propanal); and 31 amu (2-propenol).

the Cu–Pt–Pt(1 1 1) surface, there is only a weak desorption peak of CO at around 243 K and the molecular desorption of acrolein occurs at the same temperature. Hydrogenation products are not detected from the Cu–Pt–Pt(1 1 1) surface.

3.1.4. Comparison of TPD yields on different 3d/Pt(1 1 1) surfaces

Activities toward the formation of gas-phase hydrogenation and decomposition products are calculated based on the areas of TPD peaks that contribute to the cracking patterns of each gas-phase reaction product, as explained elsewhere [19]. In brief, measurements of TPD peak areas for 2-propenol, propanal, 1-propanol, ethylene, and CO were used to estimate the yields of these products from the different surfaces following the empirical procedure developed by Ko et al. [22] for the correction of mass spectrometer sensitivity. The absolute TPD yields are expressed in the unit of molecule per surface metal atom and are shown in Table 1 for the Pt–3d–Pt(1 1 1) and H/Pt–3d–Pt(1 1 1) surfaces. The sensitivity factors are calculated relative to the absolute CO coverage, which is the main product from the decarbonylation of acrolein. The absolute CO coverage was estimated by TPD following the saturation exposure of CO on clean Pt(1 1 1) [19]. The absolute yields of carbon adsorbed on the surface (C_{ads}) and H_2 were estimated based on the carbon balance considering the formation of CO from the decarbonylation and the complete decomposition of acrolein to carbonaceous species and hydrogen, as explained elsewhere [19].

As shown in Table 1, the selectivity for the hydrogenation of C=O bond to produce 2-propenol increases from ~3% to ~17% by the presence of pre-adsorbed hydrogen on the Pt–Ni–Pt(1 1 1) surface [19]. The overall yields of the main hydrogenated products from acrolein on Pt–Co–Pt(1 1 1) are similar to the ones observed on Pt–Ni–Pt(1 1 1). However, the ones on the H/Pt–Co–Pt(1 1 1) surface are smaller than those observed on the respective H/Pt–Ni–Pt(1 1 1) counterparts. Although the hydrogenation selectivity toward 2-propenol, defined as the amount of 2-propenol divided by all three hydrogenation products, is higher on H/Pt–Co–Pt(1 1 1) than on H/Pt–Ni–Pt(1 1 1), the absolute TPD yield is smaller. In comparison, the overall hydrogenated product yield on the Pt–Cu–Pt(1 1 1) surfaces is the smallest among the Pt–3d–Pt(1 1 1) surfaces shown in Table 1.

The main hydrogenated products on the 3d–Pt–Pt(1 1 1) surface structures are also calculated and reported in Table 2. Due to the absence of pre-adsorbed hydrogen, the production of propanal and 2-propenol on these surfaces is from the self-hydrogenation (disproportionation) reaction of acrolein. In general, the yield of the desirable product, 2-propenol, is lower on 3d–Pt–Pt(1 1 1) surfaces than on their subsurface counterparts. This difference becomes more obvious in the presence of pre-dosed hydrogen, which does not lead to any enhancement in the hydrogenation activity on the 3d–Pt–Pt(1 1 1) surface structures (spectra not shown).

3.2. HREELS results of acrolein on 3d/Pt(1 1 1) surfaces

In order to further understand the different reaction pathways of acrolein on the Pt–3d–Pt(1 1 1) and 3d–Pt–Pt(1 1 1) surfaces, vibrational spectra of adsorbed acrolein and its reaction intermediates were recorded after different annealing temperatures. The effect of pre-adsorbed hydrogen was also compared for several bimetallic surfaces. Due to the complexity of the HREEL spectra of acrolein and its reaction intermediates, definitive assignments of the vibrational features of the surface species would only be possible with the assistance of theoretical calculations and isotope labeling experiments, which are beyond the scope of the current paper. In the current study we will focus primarily on the interactions of the C=C and C=O bonds of acrolein and its intermediates on the different bimetallic surfaces to provide a qualitative interpretation to support the TPD results.

3.2.1. HREEL spectra of acrolein on Pt–3d–Pt(1 1 1) and 3d–Pt–Pt(1 1 1) surfaces

Fig. 4a compares the HREEL spectra after acrolein adsorption at 120 K followed by annealing to 200 K on Pt(1 1 1), Pt–Ni–Pt(1 1 1), Pt–Co–Pt(1 1 1), and Pt–Cu–Pt(1 1 1). As discussed previously, the observation of the characteristic modes of liquid-phase acrolein, ν(C=C) at 1630 cm^{-1}, ν(C=O) at 1670 cm^{-1}, and δ(CCO) at 561 cm^{-1}, indicates the presence of weakly adsorbed acrolein on Pt(1 1 1) [19]. The vibrational features are in general agreement with those observed by Loffreda et al. when acrolein is dosed on Pt(1 1 1) at around 180 K [15]. In contrast, the ν(C=C) and ν(C=O) modes are no longer well-resolved and appear as a single peak at 1644 cm^{-1} on Pt–Ni–Pt(1 1 1), suggesting that the interaction of acrolein on this surface modifies both the C=C and C=O moieties. The detection of the intense δ(CCO) at 534 cm^{-1} indicates that the skeletal bonds of acrolein remain intact on the surface. The vibrational spectra on the Pt–Co–Pt(1 1 1) and Pt–Cu–Pt(1 1 1) surfaces are in general similar to that on Pt–Ni–Pt(1 1 1), suggesting that acrolein interacts with the surfaces through both C=C and

Table 1
TPD yields for the hydrogenation of acrolein on Pt–3d–Pt(1 1 1) with and without pre-adsorbed hydrogen.

Compound	Pt(1 1 1)	Pt–Ni–Pt	H/Pt–Ni–Pt	Pt–Co–Pt	H/Pt–Co–Pt	Pt–Cu–Pt	H/Pt–Cu–Pt
$CH_3CH_2CH{=}O$	0	0.09	0.12	0.015	0.017	0.006	0.006
$CH_2{=}CHCH_2OH$	0	0.003	0.025	0.003	0.007	0.001	0.001
$CH_3CH_2CH_2OH$	0	0	0.003	0	0	0	0
CO	0.21	0.09	0.11	0.09	0.10	0.05	0.05
C_{ads}	0.35[a]	0.10[a]	0.22[a]	0.17[a]	0.20[a]	0.10[a]	0.10[a]
C_2H_4	0.03	0.04	0	0.005	0	0	
H_2	0.35[a]	0.09[a]		0.17[a]		0.10[a]	
Hydrogenation selectivity toward 2-propenol (%)	0	3	17	18	30	19	19

Values in molecule per surface Pt atom.
[a] Yields calculated from mass balance using the decarbonylation pathway.

Table 2
TPD product yields for the self-hydrogenation of acrolein on 3d–Pt–Pt(1 1 1) without pre-adsorbed hydrogen.

Compound	Ni–Pt–Pt	Co–Pt–Pt	Cu–Pt–Pt
$CH_3CH_2CH{=}O$	0.020	0.023	<0.001
$CH_2{=}CHCH_2OH$	0.002	0.002	0
$CH_3CH_2CH_2OH$	0	0	0

Values in molecule per surface Pt atom.

C=O moieties. The presence of the CO species at ~2036 cm^{-1} on all three Pt–3d–Pt(1 1 1) surfaces is from either a low temperature decarbonylation pathway or accumulation of CO from the UHV background.

In comparison, Fig. 4b shows the HREEL spectra of acrolein on the corresponding 3d–Pt–Pt(1 1 1) surfaces. The most obvious difference between Fig. 4a and b is the absence of a well-resolved δ(CCO) mode at ~534 cm^{-1} on Ni–Pt–Pt(1 1 1) and Co–Pt–Pt(1 1 1), suggesting a strong interaction between the CCO skeletal bond of acrolein with these two surfaces at 200 K. The presence of well-resolved features at 1360, 1440, and 2949 cm^{-1} on Co–Pt–Pt(1 1 1) indicates the formation of ethylidyne-type species, likely due to a low temperature decarbonylation pathway. The HREEL spectrum on Cu–Pt–Pt(1 1 1) is rather complicated, with many well-resolved features ranging from 311 to 3017 cm^{-1}, suggesting the presence of weakly adsorbed species. The absence of the ν(C=C) and ν(C=O) modes is somewhat unexpected for weakly adsorbed acrolein, although this could be due to an adsorption geometry with both the C=C and C=O bonds of acrolein parallel to the surface. Based on the TPD spectra depicted in Fig. 3, the only desorption features at greater than 200 K are unreacted acrolein (56 amu) and trace amount of CO. This in turn suggests that the vibrational features on Cu–Pt–Pt(1 1 1) in Fig. 4b are likely related to either acrolein or an intermediate that can readily combine to produce gas-phase acrolein at above 200 K.

The HREEL spectra of the surface intermediates after annealing to 300 K on Pt–3d–Pt(1 1 1) are displayed in Fig. 5a. It is important to point out that the main desorption products, other than H_2 and

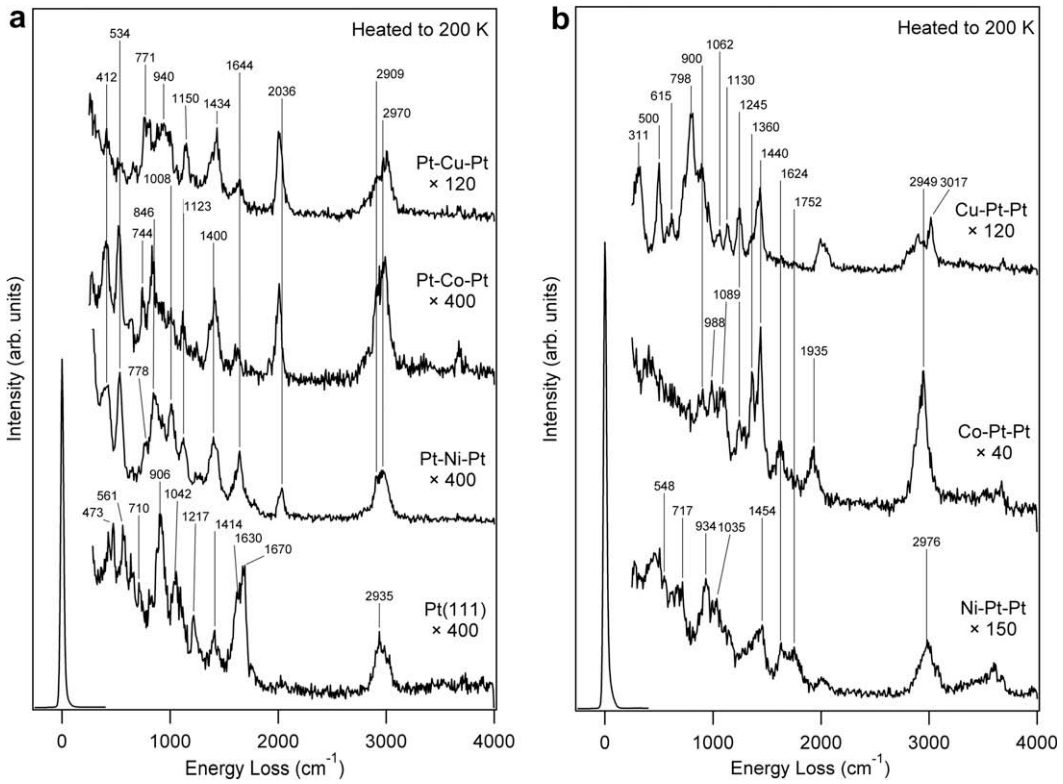

Fig. 4. (a) HREEL spectra after the adsorption of 3 L of acrolein at ~120 K followed by annealing to 200 K on Pt–3d–Pt(1 1 1); (b) HREEL spectra after the adsorption of 3 L of acrolein at ~120 K followed by annealing to 200 K on 3d–Pt–Pt(1 1 1).

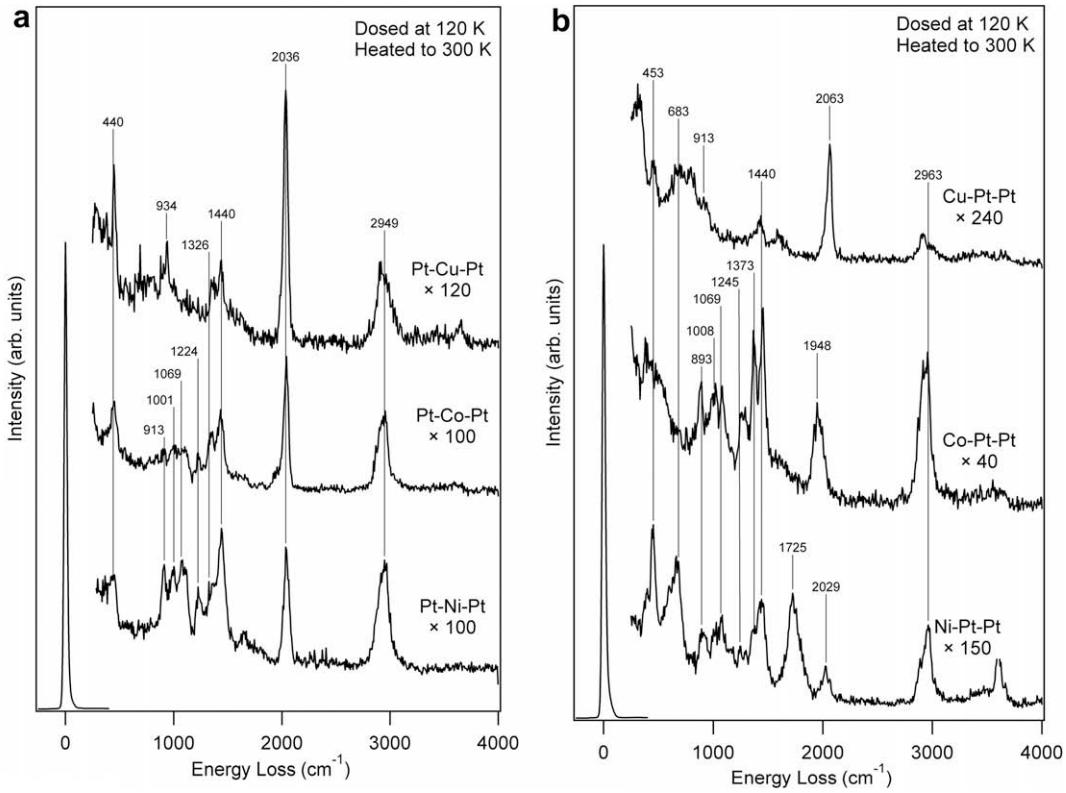

Fig. 5. (a) HREEL spectra after the adsorption of 3 L of acrolein at ~120 K followed by annealing to 300 K on Pt–3d–Pt(1 1 1); (b) HREEL spectra after the adsorption of 3 L of acrolein at ~120 K followed by annealing to 300 K on 3d–Pt–Pt(1 1 1).

CO, reach a maximum in the desorption peaks below or near 300 K. Vibrational features in the ν(C=C) and ν(C=O) regions are nearly absent at 300 K in Fig. 5a, consistent with the TPD results that acrolein and the hydrogenation products already desorbed from the surfaces by this temperature. In addition to the intense CO mode at 2036 cm^{-1}, a CH_x stretching mode is observed at 2949 cm^{-1} on all these surfaces, suggesting the presence of hydrocarbon fragments from the dissociation of acrolein. The appearance of the vibrational features at 913, 1224, 1326, 1440, and 2949 cm^{-1} indicates the presence of ethylidyne or propylidyne reaction intermediates on the surfaces.

Fig. 5b shows the vibrational features of the surface intermediates after annealing to 300 K on the corresponding 3d–Pt–Pt(1 1 1) surfaces. Unlike the subsurface Pt–Ni–Pt(1 1 1) structure, the Ni–Pt–Pt(1 1 1) surface shows an intense feature at 1725 cm^{-1}, which is likely related to the ν(C=O) mode of the propanal species or other intermediate that contains the C=O functional group, consistent with the desorption of propanal and CO from this surface at above 300 K. For the Co–Pt–Pt(1 1 1) surface, an intense CO feature is observed at 1948 cm^{-1} along with the ethylidyne-like vibrations at 913, 1069, and 1324 cm^{-1}, resulting from decarbonylation pathway. In comparison, the vibrational features on Cu–Pt–Pt(1 1 1) are not as well defined at the same annealing temperature, except the presence of an intense and sharp ν(CO) mode at 2063 cm^{-1}; the surface CO species is from the adsorption from the UHV background, instead of reaction of acrolein, based on the absence of CO desorption peak at above 300 K in the TPD measurement (Fig. 3).

The HREELS results on the Pt–3d–Pt(1 1 1) surfaces are in general consistent with the TPD data shown earlier. As expected based on the TPD results, the vibrational features on the Pt–Co–Pt(1 1 1) surface are similar to the ones observed on the Pt–Ni–Pt(1 1 1) surface at the different annealing temperatures, indicating similar hydrogenation pathways on the two surfaces. The absence of well-resolved ν(C=C) and ν(C=O) modes on the two surfaces at 200 K is consistent with the interaction of both moieties with the surface, consistent with the TPD detection of hydrogenation products via both C=C and C=O hydrogenation pathways. In comparison, the absence of the δ(CCO) mode on the Ni–Pt–Pt(1 1 1) and Co–Pt–Pt(1 1 1) surfaces at 200 K suggests a stronger interaction with adsorbed acrolein, consistent with the higher peak areas of H_2 and CO from the decomposition of acrolein. Finally, the HREELS results on the Pt–Cu–Pt(1 1 1) and Cu–Pt–Pt(1 1 1) surfaces do not resemble those of the Ni and Co counterparts, again consistent with the lower hydrogenation and decomposition activities of the Cu/Pt bimetallic surfaces in the TPD measurements.

Lastly, it is interesting to point out that there is no apparent shift in the ν(CO) mode at 2036 cm^{-1} on the three Pt–3d–Pt(1 1 1) surfaces (Fig. 5a), indicating that CO occupies the same type of metal sites, which are likely to be Pt sites modified by the presence of the 3d metals in the subsurface layer. This observation indirectly confirms that the idealized Pt–3d–Pt(1 1 1) subsurface structure is most likely produced for Ni, Co, and Cu upon the deposition of these metals on Pt(1 1 1) at 600 K. In comparison, the ν(CO) feature is observed at 2029, 1948, and 2063 cm^{-1} for the corresponding 3d–Pt–Pt(1 1 1) surfaces, further indicating the different surface composition between the surface and subsurface structures.

3.2.2. HREEL spectra of acrolein on H/Pt–Ni–Pt(1 1 1) and H/Pt–Co–Pt(1 1 1) surfaces

As summarized in Table 1, the presence of pre-adsorbed hydrogen enhances the production of 2-propenol from the Pt–Ni–Pt(1 1 1) and Pt–Co–Pt(1 1 1) surfaces. A comparison of the corresponding vibrational spectra is shown in Fig. 6. The spectra were obtained after the adsorption of acrolein on surfaces pre-dosed

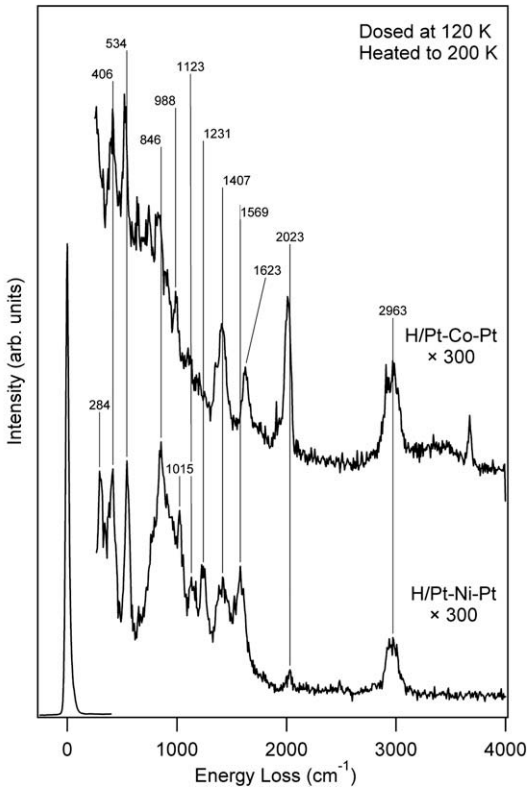

Fig. 6. HREEL spectra of the co-adsorption of 3 L of acrolein and atomic hydrogen on H/Pt–Ni–Pt(1 1 1) and H/Pt–Co–Pt(1 1 1) surfaces after annealing to 200 K.

by half saturation of hydrogen followed by annealing the surfaces to 200 K, which is below the onset temperature for the desorption of the 2-propenol product. As described in a previous paper [18], the detection of the mode at 1569 cm^{-1} on the H/Pt–Ni–Pt(1 1 1) suggests the presence of a preferred di-σ-C–O configuration for acrolein. In comparison, a vibrational feature at 1623 cm^{-1} is observed on H/Pt–Co–Pt(1 1 1), which is likely from the contribution from both the ν(C═C) and ν(C═O) modes. Such a difference in the bonding configuration of acrolein is consistent with the TPD results. The presence of pre-adsorbed hydrogen enhances the TPD yield of 2-propenol on the Pt–Ni–Pt(1 1 1) surface, which is likely due to the presence of the di-σ-C–O bonded acrolein that facilitates the hydrogenation of the C═O bond on H/Pt–Ni–Pt(1 1 1). In contrast, the TPD yield is not enhanced to the same extent by pre-adsorbed H on Pt–Co–Pt(1 1 1), which is consistent with the presence of both di-σ-C–O and di-σ-C–C species that can undergo both C═C and C═O bond hydrogenation on this surface.

3.3. General trend between Pt–3d–Pt(1 1 1) and 3d–Pt–Pt(1 1 1) surfaces

Many previous studies have utilized DFT modeling to understand the hydrogenation mechanisms of unsaturated C═C and C═O bonds [18,36–39]. In the current study, DFT calculations of binding energies of acrolein were performed to help understand the difference between the hydrogenation activities observed on the different 3d/Pt(1 1 1) surface and the subsurface structures. Table 3 shows the results for the acrolein binding energies through three different geometries, di-σ-C–C, di-σ-C–O, and η^4(C,C,C,O) on the Pt–3d–Pt(1 1 1) and 3d–Pt–Pt(1 1 1) surfaces. The binding energies of acrolein through the different geometries are similar for the Pt–3d–Pt(1 1 1) surfaces. Moreover, these calculated binding energies are very low, suggesting weak interactions of acrolein

Table 3
DFT calculations of acrolein binding energies (kJ/mol) on Pt–3d–Pt(1 1 1) and 3d–Pt–Pt(1 1 1) surfaces (3d = Ni, Co, Cu).

Surface	C–C-di-σ	C–O-di-σ	η_4
Pt–Co–Pt	−11.5	−0.4	−11.3
Pt–Ni–Pt	−13.2	−1.5	−13.9
Pt–Cu–Pt	−13.7	−1.0	−12.4
Pt	−22.7		−22.9
Cu–Pt–Pt			−24.2
Ni–Pt–Pt	−53.7		−54.0
Co–Pt–Pt			−78.1

with the subsurface structures. As reported previously for the hydrogenation of cyclohexene [40], the binding energies of atomic hydrogen on bimetallic surfaces, including all the surface and subsurface structures in the current paper, are weaker on Pt–3d–Pt(1 1 1) than on 3d–Pt–Pt(1 1 1) for any given 3d–Pt pair. In that study the hydrogenation activity was higher on Pt–3d–Pt(1 1 1) than on 3d–Pt–Pt(1 1 1) due to the fact that weaker binding energies of cyclohexene and atomic hydrogen favor the hydrogenation on the subsurface structures. Similar argument can be made in the current study for the higher hydrogenation activity of acrolein observed on Pt–3d–Pt(1 1 1) than on the corresponding 3d–Pt–Pt(1 1 1) surfaces. However, minor differences in binding energies among the three Pt–3d–Pt(1 1 1) surfaces are not sufficient to the different hydrogenation activity and selectivity on these surfaces. Weak interactions, such as the dispersive van der Waals type that are not currently possible to include in DFT, should be taken into account in a different modeling approach to better differentiate these three binding configurations. In addition, the calculation of activation barriers would be necessary for a thorough analysis and better explanation of the difference in selectivities between the different 3d/Pt(1 1 1) surfaces. As explained elsewhere, these calculations are computationally more expensive than the ones shown in this study [18].

As compared in Table 3, the three surface 3d–Pt–Pt(1 1 1) structures show higher binding energies, through either the di-σ-C–C or the η^4(C,C,C,O) configuration. The strong binding energies on the 3d–Pt–Pt(1 1 1) surfaces are most likely the origin of the lower hydrogenation activities. Furthermore, DFT results show that the di-σ-C–O configuration always converges to either di-σ-C–C or η^4(C,C,C,O) during the calculation; the absence of the di-σ-C–O configuration is consistent with the relatively low C═O bond hydrogenation activity on these surfaces.

4. Conclusions

The trends in the hydrogenation activity and selectivity of acrolein are reported here on several subsurface Pt–3d–Pt(1 1 1) and surface 3d–Pt–Pt(1 1 1) structures. The combination of TPD and HREELS experiments and DFT calculations leads to the following conclusions:

(1) TPD experiments show that a higher activity toward self-hydrogenation (disproportionation) and hydrogenation of acrolein is observed on the subsurface Pt–3d–Pt(1 1 1) structures in comparison with that observed on the corresponding surface 3d–Pt–Pt(1 1 1) structures. The highest hydrogenation activity of acrolein and yield toward the 2-propenol are observed on the H/Pt–Ni–Pt(1 1 1) surface, in agreement with the preferred di-σ-C–O adsorption mode of acrolein from the HREELS measurement.
(2) The lower hydrogenation activity to 2-propenol on the corresponding 3d–Pt–Pt(1 1 1) surface structures are related to the stronger binding energy, as well as a preferred di-σ or η^4 configuration involving the interaction of the C═C

bond of acrolein on these surfaces, which diminishes the interaction of the carbonyl group with the bimetallic surfaces. The stronger binding also favors the dissociation of the skeletal bonds of acrolein on these surfaces.

(3) Similar vibrational features are observed for the subsurfaces Pt–Co–Pt(1 1 1) and the Pt–Ni–Pt(1 1 1). This is in agreement with the general similarity in the TPD spectra for both bimetallic systems and the fact that the Pt–Co–Pt(1 1 1), with and without pre-adsorbed hydrogen, exhibits the second highest overall hydrogenation activity and yield toward 2-propenol among the bimetallic series reported in this study.

(4) Recent DFT modeling results indicate that the Pt–3d–Pt subsurface structures are thermodynamically preferred with adsorbed hydrogen [41], suggesting that surface science results from the current study should be relevant to hydrogenation activities of supported 3d–Pt bimetallic catalysts.

Acknowledgments

This work was supported by the Department of Energy, Office of Basic Energy Sciences (Grant # DE-FG02-00ER15104). We acknowledge Dr. Amit Goda for assistance in the binding energy calculations presented in Table 3.

References

[1] P. Claus, Top. Catal. 5 (1998) 51–62.
[2] P. Maki-Arvela, J. Hajek, T. Salmi, D.Y. Murzin, Appl. Catal. A – Gen. 292 (2005) 1–49.
[3] R. Hirschl, F. Delbecq, P. Sautet, J. Hafner, J. Catal. 217 (2003) 354–366.
[4] S. Galvagno, C. Milone, A. Donato, G. Neri, R. Pietropaolo, Catal. Lett. 17 (1993) 55–61.
[5] G. Neri, C. Milone, A. Donato, L. Mercadante, A.M. Visco, J. Chem. Technol. Biotechnol. 60 (1994) 83–88.
[6] C.G. Raab, J.A. Lercher, J. Mol. Catal. 75 (1992) 71–79.
[7] C.G. Raab, J.A. Lercher, Catal. Lett. 18 (1992) 99–109.
[8] M. Lucas, P. Claus, Chem. Eng. Technol. 28 (2005) 867–870.
[9] T. Birchem, C.M. Pradier, Y. Berthier, G. Cordier, J. Catal. 161 (1996) 68–77.
[10] D.I. Jerdev, A. Olivas, B.E. Koel, J. Catal. 205 (2002) 278–288.
[11] P. Beccat, J.C. Bertolini, Y. Gauthier, J. Massardier, P. Ruiz, J. Catal. 126 (1990) 451–456.
[12] F. Delbecq, P. Sautet, J. Catal. 152 (1995) 217–236.
[13] F. Delbecq, P. Sautet, J. Catal. 211 (2002) 398–406.
[14] F. Delbecq, P. Sautet, J. Catal. 220 (2003) 115–126.
[15] D. Loffreda, Y. Jugnet, F. Delbecq, J.C. Bertolini, P. Sautet, J. Phys. Chem. B 108 (2004) 9085–9093.
[16] D. Loffreda, F. Delbecq, V. Fabienne, P. Sautet, Angew. Chem. Int. Ed. 44 (2005) 5279–5282.
[17] D. Loffreda, F. Delbecq, V. Fabienne, P. Sautet, J. Am. Chem. Soc. 128 (2006) 1316–1323.
[18] L.E. Murillo, A.M. Goda, J.G. Chen, J. Am. Chem. Soc. 129 (2007) 7101–7105.
[19] L.E. Murillo, J.G. Chen, Surf. Sci. 602 (2008) 919–931.
[20] L.E. Murillo, J.G. Chen, Surf. Sci. 602 (2008) 2412–2420.
[21] N.A. Khan, H.H. Hwu, J.G. Chen, J. Catal. 205 (2002) 259–265.
[22] E.I. Ko, J.B. Benziger, R.J. Madix, J. Catal. 62 (1980) 264–274.
[23] H.H. Hwu, J.G. Chen, J. Phys. Chem. B 107 (2003) 2029–2039.
[24] N. Liu, S.A. Rykov, J.G. Chen, Surf. Sci. 487 (2001) 107–117.
[25] J.R. Kitchin, N.A. Khan, M.A. Barteau, J.G. Chen, B. Yakshinksiy, T.E. Madey, Surf. Sci. 544 (2003) 295–308.
[26] G. Kresse, J. Furthmuller, Phys. Rev. B 54 (1996) 11.
[27] C.A. Menning, H.H. Hwu, J.G. Chen, J. Phys. Chem. B 110 (2006) 15471–15477.
[28] J.G. Chen, C.A. Menning, M.B. Zellner, Surf. Sci. Rep. 63 (2008) 201–254.
[29] J.C. de Jesus, F. Zaera, Surf. Sci. 430 (1999) 99–115.
[30] P. Grutter, U.T. Durig, Phys. Rev. B 49 (1994) 2021–2029.
[31] J.S. Tsay, C.S. Shern, Surf. Sci. 396 (1998) 313–318.
[32] Y. Gauthier, M. Schmid, S. Padovani, E. Lundgren, V. Bus, G. Kresse, J. Redinger, P. Varga, Phys. Rev. Lett. 87 (2001) 036103-1–036103-4.
[33] N.A. Khan, L.E. Murillo, J.G. Chen, J. Phys. Chem. B 108 (2004) 15748–15754.
[34] O. Skoplyak, M.A. Barteau, J.G. Chen, J. Phys. Chem. B (2006) 1686–1694.
[35] J.S. Tsay, T. Mangen, R.-J. Linden, K. Wandelt, Surf. Sci. 482–485 (2001) 866–871.
[36] V. Pallassana, M. Neurock, J. Catal. 191 (2000) 301–317.
[37] V. Pallassana, M. Neurock, J. Phys. Chem. B 104 (2000) 9449–9459.
[38] F. Delbecq, F. Vigne-Maeder, C. Becker, J. Breitbach, K. Wandelt, J. Phys. Chem. C 112 (2008) 555.
[39] M.P. Humbert, L.E. Murillo, J.G. Chen, ChemPhysChem 9 (2008) 1262–1264.
[40] M.P. Humbert, J.G. Chen, J. Catal. 257 (2008) 297–306.
[41] C.A. Menning, J.G. Chen, J. Chem. Phys. 128 (2008) 164703.